

# Lawrence Berkeley National Laboratory

## LBL Publications

### Title

Warming and Increased Respiration Have Transformed an Alpine Steppe Ecosystem on the Tibetan Plateau From a Carbon Dioxide Sink Into a Source

### Permalink

<https://escholarship.org/uc/item/9v67w6c1>

### Journal

Journal of Geophysical Research Biogeosciences, 127(1)

### ISSN

2169-8953

### Authors

Yun, Hanbo  
Tang, Jing  
D'Imperio, Ludovica  
[et al.](#)

### Publication Date

2022

### DOI

10.1029/2021jg006406

### Copyright Information

This work is made available under the terms of a Creative Commons Attribution-NonCommercial License, available at <https://creativecommons.org/licenses/by-nc/4.0/>

Peer reviewed

1 Warming and increased respiration have transformed an alpine steppe ecosystem  
2 on the Tibetan Plateau from a carbon dioxide sink into a source

3 Hanbo Yun<sup>1,2,3</sup>, Jing Tang<sup>4</sup>, Ludovica D'Imperio<sup>2</sup>, Xiaobo Wang<sup>5</sup>, Yang Qu<sup>6</sup>, Licheng Liu<sup>7</sup>,  
4 Qianlai Zhuang<sup>3</sup>, Wenxin Zhang<sup>2,4</sup>, Qingbai Wu<sup>1\*</sup>, Anping Chen<sup>8\*</sup>, Qing Zhu<sup>9</sup>, Deliang Chen<sup>10</sup>,  
5 Bo Elberling<sup>2\*</sup>

6

7

8 <sup>1</sup>State Key Laboratory of Frozen Soil Engineering, Northwest Institute of Eco--Environment and  
9 Resources, Chinese Academy of Sciences, Lanzhou, Gansu 730000, China

10 <sup>2</sup>Center for Permafrost (CENPERM), Department of Geosciences and Natural Resource  
11 Management, University of Copenhagen, DK1350 Copenhagen, Denmark

12 <sup>3</sup>Department of Earth, Atmospheric and Planetary Sciences, Purdue University, West Lafayette,  
13 Indiana 47906, USA

14 <sup>4</sup>Department of Physical Geography and Ecosystem Science, Lund University, SE--22236 Lund,  
15 Sweden

16 <sup>5</sup>Key Laboratory of Ecohydrology of Inland River Basin, Northwest Institute of Eco--  
17 Environment and Resources, Chinese Academy of Sciences, Lanzhou, Gansu 730000, China

18 <sup>6</sup>School of Urban and Regional Science, East China Normal University, Shanghai 200062, China

19 <sup>7</sup>Department of Bioproducts and Biosystems Engineering, University of Minnesota, St Paul, MN,  
20 USA

21 <sup>8</sup>Department of Biology and Graduate Degree Program in Ecology, Colorado State University,

22 Fort Collins, Colorado 80523, USA

23 <sup>9</sup>Climate Sciences Department, Climate and Ecosystem Sciences Division, Lawrence Berkeley

24 National Laboratory, 94720 Berkeley, California, USA

25 <sup>10</sup>Department of Earth Sciences, University of Gothenburg, 41320 Gothenburg, Sweden

26

27 \*Authors for correspondence: qbwu@lzb.ac.cn (QW), apchen1111@gmail.com(AC),

28 be@ign.ku.dk (BE)

29

30

31

32

33

34

35

36

Manuscript accepted to *Journal of Geophysical Research -- Biogeosciences*

37

38

39

40

41 **Plain Language Summary:**

42

43 Cold region ecosystems store vast amounts of soil organic carbon (SOC), which upon warming and  
44 decomposition can affect the net carbon balance and potentially change these ecosystems to become a  
45 source of carbon dioxide (CO<sub>2</sub>) to the atmosphere. We have measured year-round CO<sub>2</sub> fluxes over 10  
46 years from an alpine steppe-ecosystem on the Tibetan Plateau. The results show that the region has  
47 experienced pronounced warming during the study period and that the resulting near-surface soil  
48 warming is a key parameter for explain why the ecosystem over 10 years have changed from being a net  
49 sink to become a net source of CO<sub>2</sub> to the atmosphere. Measurements year-round demonstrate that the  
50 shift in the CO<sub>2</sub> balance is mainly due to a marked increase in decomposition of SOC during the non-  
51 growing-season. Furthermore, observations reveal several high-emission events at the end of the non-  
52 growing season and early in the growing season, which have increased in importance during the study  
53 period. The results are important to improve our understanding of the sensitivity of cold ecosystem  
54 respiration to warming and to highlight the importance of winter processes and emissions events on the  
55 annual ecosystem carbon budget.

56

57 **Three main key points:**

(1) Warming of the Tibetan Plateau has consequences for the net carbon balance

(2) Significant warming has resulted in a net carbon loss from soil respiration

(3) The steppe-ecosystem has changed from being a sink to a source of CO<sub>2</sub> to the atmosphere

58

59

60

61

62 **Abstract**

63 Cold region ecosystems store vast amounts of soil organic carbon (C), which upon warming and  
64 decomposition can affect the C balance and potentially change these ecosystems from C sinks to  
65 carbon dioxide (CO<sub>2</sub>) sources. We quantified the decadal year-round CO<sub>2</sub> flux from an alpine  
66 steppe-ecosystem on the Tibetan Plateau using eddy covariance and automatic chamber  
67 approaches during a period of significant warming (0.13°C per 10 years; and 0.18°C in the non-  
68 growing season alone: 1<sup>st</sup> October to next 30<sup>th</sup> April). The results showed that ongoing climate  
69 change, mainly warming within the topsoil layers, is the main reason for the site's change from a  
70 sink for to a source of CO<sub>2</sub> in the atmosphere. Non-growing-season ecosystem respiration  
71 accounted for 51% of the annual ecosystem respiration and has increased significantly. The  
72 growing seasons (1<sup>st</sup> May to 30<sup>th</sup> September) were consistent CO<sub>2</sub> sink periods without  
73 significant changes over the study period. Observations revealed high-emission events from the  
74 end of the non-growing season to early in the growing season (1<sup>st</sup> March to 15<sup>th</sup> May), which  
75 significantly ( $p < 0.01$ ) increased at a rate of 22.6 g C m<sup>-2</sup> decade<sup>-1</sup>, ranging from 14.6 ± 10.7 g  
76 C m<sup>-2</sup> yr<sup>-1</sup> in 2012 to 35.3 ± 12.1g C m<sup>-2</sup> yr<sup>-1</sup> in 2017. Structural equation modelling suggested  
77 that active layer warming was the key factor in explaining changes in ecosystem respiration  
78 leading to significant changes in net ecosystem exchange over the period 2011-2020 and  
79 indicated that these changes have already transformed the ecosystem from a CO<sub>2</sub> sink into a  
80 source. These results can be used to improve our understanding of the sensitivity of ecosystem  
81 respiration to increased warming during the non-growing period.

82

## 83 **1. Introduction**

84 The Northern Hemisphere permafrost region stores carbon (C) as soil organic C equal to roughly  
85 twice the amount present in the atmosphere (Hugelius et al., 2013). The net ecosystem exchange  
86 of carbon dioxide (CO<sub>2</sub>) depends on the balance of decomposition of soil C reserves and the  
87 fixation of atmospheric CO<sub>2</sub> by vegetation (Euskirchen et al., 2017; Davidson & Janssens, 2006).  
88 Warming of the active layer (AL, defined as the portion of the soil profiles thawing each  
89 summer) and thawing of previously-frozen soils can stimulate soil organic matter decomposition  
90 and thus increase ecosystem heterotrophic respiration, leading to a positive feedback in terms of  
91 atmospheric CO<sub>2</sub> concentration (Schuur et al., 2009; Elberling et al., 2013; Plaza et al., 2020). In  
92 contrast, wetter conditions and changes in oxygen availability in the soil may lead to reduced  
93 respiration rates and consequently increased protection of the soil C reserves (Elberling et al.,  
94 2013; Schuur et al., 2021). Moreover, the combination of warming, increasing soil moisture and  
95 higher atmospheric CO<sub>2</sub> concentrations can also increase net primary production (NPP) through  
96 enhancing plant productivity (Epstein et al., 2012) and change the plant community composition  
97 (Zhu et al., 2016; Bjorkman et al., 2018).

98 There is still no consensus among observational and modelling studies with respect to  
99 permafrost-affected ecosystems functioning as a net CO<sub>2</sub> sink or source (Celis et al., 2017;  
100 Zhang et al., 2018). Most studies agree that tundra ecosystems over the past 100-1000 years have  
101 functioned as net CO<sub>2</sub> sink areas (Prik et al., 2017; Min et al., 2021). However, site-specific  
102 studies have shown that tundra can function as either a net CO<sub>2</sub> source or sink under recent  
103 climate warming (Oechel et al., 2000; Schuur et al., 2015; Lupascu et al., 2014; Wickland et al.,  
104 2020). A recent review demonstrated that across 148 terrestrial high-latitude sites, the net  
105 ecosystem exchange (NEE) in the period 1990--2015 indicated that the region was on average an

106 annual CO<sub>2</sub> sink although uncertainty remains high (Vikkala et al., 2021). All of these studies  
107 mainly focus on the Arctic (high-latitude) permafrost region and are rarely extended to high  
108 altitudes (Ding et al., 2016). Therefore, it remains unclear whether the underlying mechanisms  
109 and processes found at high latitudes also apply to high-altitude regions (Yun et al., 2018).

110 The Tibetan Plateau has the largest extent of high-altitude permafrost in the world (Chen et al.,  
111 2015) and has experienced pronounced warming, wetting and permafrost degradation over recent  
112 decades (Yao et al., 2016). The environmental changes and alteration of ecosystem C processes  
113 could lead to changes in CO<sub>2</sub> flux (Yun et al., 2018; Wei et al., 2021). This study examined the  
114 temporal variations and trends of ecosystem CO<sub>2</sub> exchange by combining plot-scale (< 1 m<sup>2</sup> by  
115 automatic chambers) and landscape (> 10,000 m<sup>2</sup> by EC) CO<sub>2</sub> measurement data at an  
116 experimental site in the Tibetan Plateau. The site is known to be a C sink area (Piao et al., 2019)  
117 but is currently subject to marked warming (Wu et al., 2015). The present study is based on the  
118 following hypotheses: (1) ecosystem respiration will be controlled by both warming and changes  
119 in soil moisture. Therefore, an increase in ecosystem respiration is expected during warm periods  
120 if changes in soil moisture are not limiting the availability of water (too dry) or oxygen (too wet);  
121 (2) warming and changes in soil moisture will similarly regulate plant growth and thereby  
122 influence NEE; (3) the net effect of plant growth and respiration on NEE is expected to vary  
123 from year to year and only measurements made across multiple years will allow a sensitivity  
124 analysis of NEE with respect to environmental factors as well as robust measures of current CO<sub>2</sub>  
125 sink/source capacity. Answering these questions will help us to understand how alpine steppe  
126 ecosystems respond to climate-induced warming on the Tibetan Plateau, and ultimately to predict  
127 the potential changes in ecosystem carbon balance.

128



## 129 2. Methods

### 130 2.1. Site descriptions and setup

131 This study was conducted near the Beilu'He research station located in a representative  
132 permafrost region (Niu et al., 2019) on the Tibetan Plateau (34°09'06"N, 92°02'57"E;  
133 Supplementary Fig. S1), with an altitude of about 4670 m. From 2010 to 2020, the mean annual  
134 temperature varied from -3.1 to -2.3°C, the mean annual precipitation ranging between 287.4 and  
135 440.8 mm and the Palmer aridity index ranging from 0.4 to 0.6 (Ding et al., 2017). The dominant  
136 vegetation type is alpine steppe with the following corresponding dominant species: *Carex*  
137 *moorcroftii* Falc. ex Boott, *Kobresia tibetica* Maxim and *androsace tanggulashanensis*, and *Rhodiola*  
138 *tibetica*. The mean plant height was  $13.7 \pm 4.6$  cm and the mean rooting depth was  $21.2 \pm 5.4$  cm.  
139 Two dwarf deciduous shrubs (*Potentilla parvifolia* Fisch. ex. Lehm. and *Myricaria prostrata*  
140 *Hook. f. et Thoms. ex Benth*) were first identified in 2013 (Yun et al., 2018). The aboveground  
141 and belowground (0-100 cm) biomasses ranging from  $108.2 \pm 30.8$  to  $124.5 \pm 42.5$  g m<sup>-2</sup> and  
142  $2427.0 \pm 61.9$  to  $2710.3 \pm 47.1$  g m<sup>-2</sup>, respectively. The main soil type is Inceptisol (Soil  
143 Taxonomy; USDA, 1999) or Cambisol (World Reference Base for Soil Resources; IUSS  
144 Working Group WRB, 2014). The main body of the permafrost was formed during the late  
145 Pleistocene Last Glaciation Maximum (26,500-19,000 years BP; Zhou et al., 2000), but  
146 experienced extensive degradation after the warming period during the Holocene (8,500-4,000  
147 years BP; Jin et al., 2007). Subsequently, new permafrost formed during the Neoglaciation  
148 period (4,000-1,000 years BP; Jin et al., 2007). Currently, the average active layer thickness is  
149 ~1.9 m (Cheng et al., 2019) and increased at a rate of  $>1.3$  cm yr<sup>-1</sup> from 1995 to 2007 (Wu &  
150 Zhang, 2010).

151 The EC-based CO<sub>2</sub> fluxes were measured from July 2010 to December 2020. The CO<sub>2</sub> fluxes  
152 were simultaneously measured at the plot level (100 cm × 100 cm) using automatic chambers,  
153 with the first measurement beginning in May 2012. The automatic chamber plots were located  
154 just outside the tower fetch, within the EC footprint area with a similar vegetation community  
155 and similar soil and climatic conditions.

156

## 157 **2.2. Environmental Monitoring**

158 A Campbell weather station (Campbell, Salt Lake City, USA) was used to monitor the  
159 environmental parameters and was installed on a 10 m mast and placed about 1.3 km away from  
160 the EC tower. Air temperature, air pressure and air humidity were measured 3 m above the  
161 ground, with precisions of ± 0.1 °C and 0.1%, respectively (HMP45C, Vaisala Inc., Finland).  
162 Incident and net radiation were monitored by a four-component net radiometer (Rn; CNR-1,  
163 Netherlands), mounted on the tower 3 m above the soil surface. The wind direction and wind  
164 speed were measured 3 m above the ground with a propeller anemometer (P2546, Campbell, Salt  
165 Lake City, USA). Half-hourly interval data were automatically recorded with a data logger  
166 (CR3000, Campbell, Salt Lake City, USA). Soil heat flux was monitored by two pre--calibrating  
167 soil heat flux sensors (HFP01, Netherlands) and inserted 5 and 15 cm below the ground. Air  
168 pressure was measured by a CS100 barometer (CS100, Campbell, Salt Lake City, USA).  
169 The temperature of the permafrost was continuously monitored using two permafrost boreholes  
170 by constantan-copper thermocouples at 50 cm intervals to a total depth of 50 and 100 m and  
171 adjacent to the EC tower. Soil temperature and soil water tensions were monitored near the  
172 micrometeorological tower with a group of pF-meter sensors (soil temperature and soil water  
173 tension precision were ± 0.25°C and ± 0.05, respectively; GEO -Precision, Germany), at 10 cm

174 resolution in the upper 100 cm and 50 cm intervals to a depth of 550 cm. An additional 10 cm  
175 resolution was obtained near the former permafrost table from 150 to 300 cm depth. Precipitation  
176 was monitored with a TE525MM rain gauge (precision is  $\pm 0.1$  mm; Texas Electronics Inc.,  
177 USA). All data were measured every 5 minutes and averaged at half-hour intervals, recorded  
178 with data logger CR3000 (Campbell, Salt Lake City, USA). Soil temperature data from two  
179 different sensors were calibrated by the Meteorological Data Service Center, the State Key  
180 Laboratory of Frozen Soil Engineering, China.

181 Soil physical and chemical properties of 240 soil and sediment samples collected within 100 m  
182 of the EC tower were analysed at the State Key Laboratory of Frozen Soil Engineering, China.  
183 Topsoil samples (0-100 cm) were sampled using a soil corer (5 cm diameter) at 10 cm intervals.  
184 For samples below 100 cm we used a motorized drill to collect samples at 50 -cm intervals to a  
185 depth of 500 cm in the middle of September every year from 2008 to 2020. The samples were  
186 collected using a stainless--steel ring cutter with three replicates. The permafrost table was  
187 determined by the ice content of the core sampling. All samples were marked and sealed in a 100  
188 ml steel aluminium box, weighed, frozen at  $-15$  °C, and brought back to the laboratory. The SOC  
189 of the air-dried soil samples was analysed using the wet combustion method, Walkley-Black  
190 modified acid dichromate digestion,  $\text{FeSO}_4$  titration and an automatic titrator. TN was measured  
191 by an elemental analyser (Vario EL Three, Elementar, Germany). The soil C:N ratio was then  
192 calculated as the quotient of the SOC and the TN concentration. The soil pH level was  
193 determined by amperometry (DJS-1C, Leizi, Shanghai, China).

194

195

196

197 **2.3. Carbon dioxide flux measurements**

198 Net ecosystem exchange (NEE) was monitored by the automatic chambers at the plot scale and  
199 by the eddy covariance tower (EC) at the landscape scale. Here, the positive (+) and negative (-)  
200 values of the CO<sub>2</sub> fluxes represent net ecosystem carbon emission and net carbon uptake,  
201 respectively.

202

203 **2.3.1 Automatic chamber setup**

204 The ecosystem NEE ( $\mu\text{mol C m}^{-2} \text{ s}^{-1}$ ) and respiration ( $R_{\text{eco}}$ ,  $\mu\text{mol C m}^{-2} \text{ s}^{-1}$ ) were measured  
205 using three translucent chambers and three dark chambers equipped with an automated CO<sub>2</sub> flux  
206 chamber system (Li-Cor 8100 extended by Li-Cor 8150, USA) at six different locations. From 1<sup>st</sup>  
207 May to 30<sup>th</sup> September, the chamber was set to measure at a rate of 5 min h<sup>-1</sup> and from 1<sup>st</sup>  
208 October to 30<sup>th</sup> April, it was set to measure at 10 min h<sup>-1</sup>. Air temperature, air pressure, moisture  
209 and CO<sub>2</sub> concentrations within the chamber and CO<sub>2</sub> concentrations in the atmosphere were  
210 recorded using a Li-Cor 8100. The chamber NEE data were expressed as  $\mu\text{mol CO}_2 \text{ m}^{-2} \text{ s}^{-1}$  using  
211 the plot-specific chamber air pressure, air temperatures and chamber volume. The flux data were  
212 then screened for any equipment failure, power outage and/or any unsuitable environmental  
213 conditions producing erratic fluxes (such as wind speeds exceeding 10 m s<sup>-1</sup>). After screening,  
214 about 83% of total flux measurements were used for further analysis. A more detailed description  
215 of the data processing can be found in Mauritz et al. (2017).

216

217 **2.3.2 Eddy covariance setup**

218 The NEE was also directly measured by the EC tower. The EC system was mounted at a 3 m  
219 height, including a sonic anemometer (CSAT3, Campbell, Salt Lake City, USA) and an open

220 path infrared gas analyser (LI-7500A, LI-COR Biosciences, USA). In July 2017, the open path  
221 infrared gas analyser was updated to LI-7500RS (LI-COR Biosciences, USA). The data for wind,  
222 CO<sub>2</sub>, water vapour and air temperature were recorded by the LI-COR 7550 analyser (LI-COR  
223 Biosciences, USA). The measurements with the LI-7500A and LI-7500RS analysers, including  
224 CO<sub>2</sub>, water vapour and dew point, were calibrated by the China Land-Atmosphere Coordinated  
225 Observation System. Fluxes were computed from the covariance of CO<sub>2</sub> and vertical wind speed  
226 using Eddypro 6.2.0 (Li-Cor Biosciences, USA) and reported as an average over 30-minute  
227 intervals.

228 The tilt correction algorithm was adopted for the correction of wind resulting from any sonic  
229 anemometer misalignment in terms of local wind streamlines (Wilczak et al., 2001). Here, the  
230 fluxes were corrected using the wind axis double rotation method (Aubinet et al., 1999) and then  
231 corrected by time lag with covariance maximization, air density, frequency loss and sensor  
232 separation according to Burba et al. (2012), with statistical testing following Vickers and Mahrt  
233 (1997), including accepted spikes at a threshold of  $\leq 1\%$  and if spikes  $> 1\%$ , they were excluded  
234 and replaced with new data by linear interpolation. The plausible ranges of wind were five  
235 standard deviations (SD), whereas those for water (H<sub>2</sub>O) and CO<sub>2</sub> were 3.5 SD. Post-field data  
236 processing included data (1) that contained any missing data points, (2) where friction velocity  
237 ( $U^*$ ) was smaller than  $0.10 \text{ m s}^{-1}$  (Goulden et al., 1996), or (3) where standard deviation of the  
238 orthogonal wind components was greater than one sigma from the mean. In contrast to LI-7500,  
239 the two analysers used here, LI-7500A/RS, did not need any corrections to account for additional  
240 instrument-related sensible heat flux according to the instruction manual for Eddypro 9.0.  
241 Data QA/QC flagging was based on developed turbulence tests and steady states, giving three  
242 levels of data quality, where 0 indicated high (58% in this study), 1 indicated intermediate (19%)

243 and 2 indicated poor quality data (18%, not including missing data, which accounted for 5% of  
244 the total data), which were discarded when calculating the yearly and seasonal C budgets (Belshe  
245 et al., 2012; Yun et al., 2018). The footprint of the EC tower ranging from 115 to 172 m,  
246 estimated based on the method of Kljun et al. (2015), which covered a similar vegetation and  
247 permafrost state. The surface energy balance ratio (EBR) was calculated based on the method of  
248 Wilson et al. (2002). The mean EBR value was about 0.68, which is within the range given by  
249 the global FLUXNET (from 0.34 to 1.69; Wilson et al., 2002).

250

#### 251 **2.4. Gap filling and budget calculations**

252 Based on growing degree days (GDD) and phenology recorded from 1975 to 2020, Beilu'He  
253 Station's growing season starts around 10<sup>th</sup> May and ends on 30<sup>th</sup> September. Thus, the  
254 subsequent non-growing season starts around 1<sup>st</sup> October and ends on 9<sup>th</sup> May. In order to enable  
255 comparison with other studies, the growing season is in the following defined as the period  
256 between 1<sup>st</sup> May and 30<sup>th</sup> September while 1<sup>st</sup> October to 30<sup>th</sup> April is considered the non-  
257 growing season.

258 Missing data from the EC tower due to harsh weather conditions and power issues represent 23%  
259 of the data gathered over the entire study period, which were subsequently filled using growing  
260 season- and non-growing season-specific models (Tovi Data Analysis software, Li-Cor  
261 Biosciences, USA). For auto-chambers, there was a 17% data gap for CO<sub>2</sub> fluxes over the whole  
262 period. All CO<sub>2</sub> fluxes were measured and gap-filled at 30-minute intervals and then aggregated  
263 to daily, seasonal and annual sums.

264 Uncertainties regarding the gap-filled EC data were assessed by bootstrapping to determine the  
265 difference between measured mean value and standard deviation (SD). Correlation regression

266 studies were done to determine the difference between the gap-filled and measured EC data; the  
267 significance level was  $P < 0.05$ . In each category, artificial data sets were created by adding  
268 predicted model values to randomly drawn and replaced residuals and models were refit in order  
269 to gap-fill data. The 95% confidence interval was obtained from 1000 complete flux time series  
270 for seasonal cumulative fluxes. Auto-chamber uncertainties were based on SD of replicate plot  
271 measurements,  $n=6$ .

272

#### 273 **2.4.1. Growing season gap filling**

274 In daytime, the gaps in EC-based NEE data were filled using the hyperbolic light response  
275 equation when the PAR values were higher than  $10 \mu\text{mol m}^{-2} \text{s}^{-1}$  (Thornley & Johnson, 1990).  
276 For the automatic chambers, hyperbolic light response curves were generated for each individual  
277 plot and were then used to gap-fill the NEE data on a monthly basis. For night-time NEE, the  
278 gaps ( $R_{\text{eco}}$ ,  $\text{PAR} < 10 \mu\text{mol m}^{-2} \text{s}^{-1}$ ) were filled using the exponential temperature response  
279 curves together with the soil temperature of 10 cm for the automatic chamber and the air  
280 temperature 3 m from the EC system. The Q10 value used for temperature responses of  
281 ecosystem respiration was 4.3 (Chen et al., 2016), derived from night-time NEE temperature  
282 responses. The correlation regression fit result show that the  $p < 0.01$ ,  $R^2 = 0.84$ ,  $\text{RMSE} = 3.37$   
283 (root mean square error) between mean value of model gap-filled data and EC measured data,  
284 whereas the  $p < 0.01$ ,  $R^2 = 0.91$ ,  $\text{RMSE} = 1.57$  for the automatic chamber. The gross ecosystem  
285 primary productivity (GPP) was estimated by subtracting  $R_{\text{eco}}$  from NEE.

286

287

288

#### 289 **2.4.2. Non-growing season gap-filling**

290 Non-growing season gap-filling and cumulative CO<sub>2</sub> flux assessment were divided into autumn  
291 (October), winter (November to -January) and spring (February to April). This study accounts for  
292 GPP in the autumn (October) and spring (February to April). Potential impacts from the  
293 lengthened growing season on the measured CO<sub>2</sub> fluxes has previously been discussed (Ueyama  
294 et al., 2014; Zhu et al., 2020).

295 In the autumn (October) and spring (February to April), for the chamber, NEE and R<sub>eco</sub> were  
296 fitted using response curves to weekly light and temperature. R<sub>eco</sub> in spring (February to April)  
297 was estimated using the winter model for both automatic chambers and EC, as soils were frozen.  
298 The NEE for spring (February to April) was analysed based on the sum of GPP and R<sub>eco</sub> (Webb  
299 et al., 2016). For the EC, autumn (October) and spring (February to April) NEE were computed  
300 weekly where GPP could be detected. R<sub>eco</sub> fluxes in winter (November to January) were gap-  
301 filled based on the exponential relationship between NEE and soil temperature of 0-30 cm. The  
302 correlation regression fit result show that the  $p < 0.01$ ,  $R^2 = 0.87$ , RMSE= 2.65 between mean  
303 value of model gap-filled data and EC measured data, whereas the  $p < 0.01$ ,  $R^2 = 0.94$ , RMSE=  
304 1.18 for the automatic chamber.

305

#### 306 **2.5. Data analysis**

307 The differences at annual, growing season and non-growing season time scale NEE/GPP/Reco  
308 were used bootstrapped to calculate the mean (95% confidence interval) to test for significant  
309 difference. For the auto-chamber, similar seasonal differences have been analysed using a *post-*  
310 *hoc Tukey test* and ANOVA. Bootstrapping, a *post-hoc Tukey test*, and ANOVA were  
311 implemented using R 3.6.3 (R Development Core team, 2020) and the significant level of alpha



312 tested based on an acceptable level of 0.05. Correlation analyses were conducted to examine the  
313 relationships between NEE and environmental factors, the thickness of the active layer and  
314 monthly soil properties during the growing season. Soil properties included soil organic carbon  
315 (SOC) content, carbon-to-nitrogen ratio (C/N) and soil pH. All of the above data of the Beilu'He  
316 station during the observation period were obtained from the State Key Laboratory of Frozen  
317 Soil Engineering and the measurement of the data was detailed in Yun et al. (2018) as well as the  
318 NEE of the non-growing season with the above-mentioned variables. All data are presented as  
319 mean values with standard deviations (SD) and the confidence interval is 95%.

320 Structural equation modelling (SEM) was conducted to quantify the direct and indirect processes  
321 in regulating NEE at different seasonal intervals (annual, growing season and non-growing  
322 season). SEM is a multivariate statistical analysis technique and in the model, the hypothetical  
323 pathways of influence between different variables can be designed and tested based on our  
324 understanding of process interactions (Miao et al., 2009). This technique goes beyond traditional  
325 multivariate techniques by integrating knowledge-based interactions among different variables  
326 (Grace, 2006).

327 To investigate seasonal differences in the underlying mechanisms that drive the interannual  
328 variations of NEE, two SEMs were constructed for the growing season and non-growing season  
329 separately. Model construction and model optimization were carried out to obtain the final SEM.  
330 In this study, driving variables were only included if they were significantly correlated with the  
331 response variable in the model, which was done through the correlation analysis between  
332 different driving variables and the response variable (NEE; Supplementary Table 1).

333 Subsequently, different pathways between these driving variables and the response variable were  
334 designed. The CO<sub>2</sub> flux uptake or release in the permafrost-affected ecosystem and permafrost

335 warming (i.e., the thickness of the active layer) were assumed to play direct roles in the NEE  
336 process. Furthermore, environmental factors (i.e., soil temperature and soil water content, air  
337 temperature, vapour pressure deficit, net radiation) can have a direct effect on NEE, as we  
338 presumed that soil properties can directly/indirectly impact NEE. Given that GPP and  $R_{\text{eco}}$  were  
339 modelled by the NEE observation, the GPP and  $R_{\text{eco}}$  were not used in the SEM calculations.  
340 The model was iteratively optimized based on the measurement data over the same periods,  
341 following Colman and Schimel (2013), by gradually removing pathways with  $P > 0.05$ . The chi-  
342 square statistic ( $\chi^2$ ) and the root-mean-square error of approximation (RMSEA) were used to  
343 assess the overall goodness of each model (Grace et al., 2006; Asparouhov et al., 2018). A  
344 normal distribution test was performed using the Kolmogorov-Smirnov method for all the data  
345 and the unnormal distributed data were transformed to normal using a logarithmic function. SEM  
346 and related statistical analyses were performed using the software R version 3.6.3 with the ‘sem’  
347 and ‘stats’ packages.

348

### 349 **3. Results**

#### 350 **3.1. Environmental conditions**

351 Annual mean air temperature measured at 3 m was  $-3.5 \pm 1.7^\circ\text{C}$  (result  $\pm$  SD) for the  
352 measurement period (2010-2020), which is significantly higher than that for the period of 1975-  
353 2020 (hereafter described as ‘long-term’,  $-4.2 \pm 2.2^\circ\text{C}$ ) for this region (Table 1). Air  
354 temperatures during the growing seasons were of similar magnitude to the long-term mean for  
355 this region ( $4.0 \pm 1.6$  vs  $3.9 \pm 3.2^\circ\text{C}$ ). However, for the non-growing season, air temperature of  
356 the period 2010-2020 was significantly higher than the long-term mean. Mean air temperature  
357 warming was significant both for the non-growing season and annual in the period 2010-2020

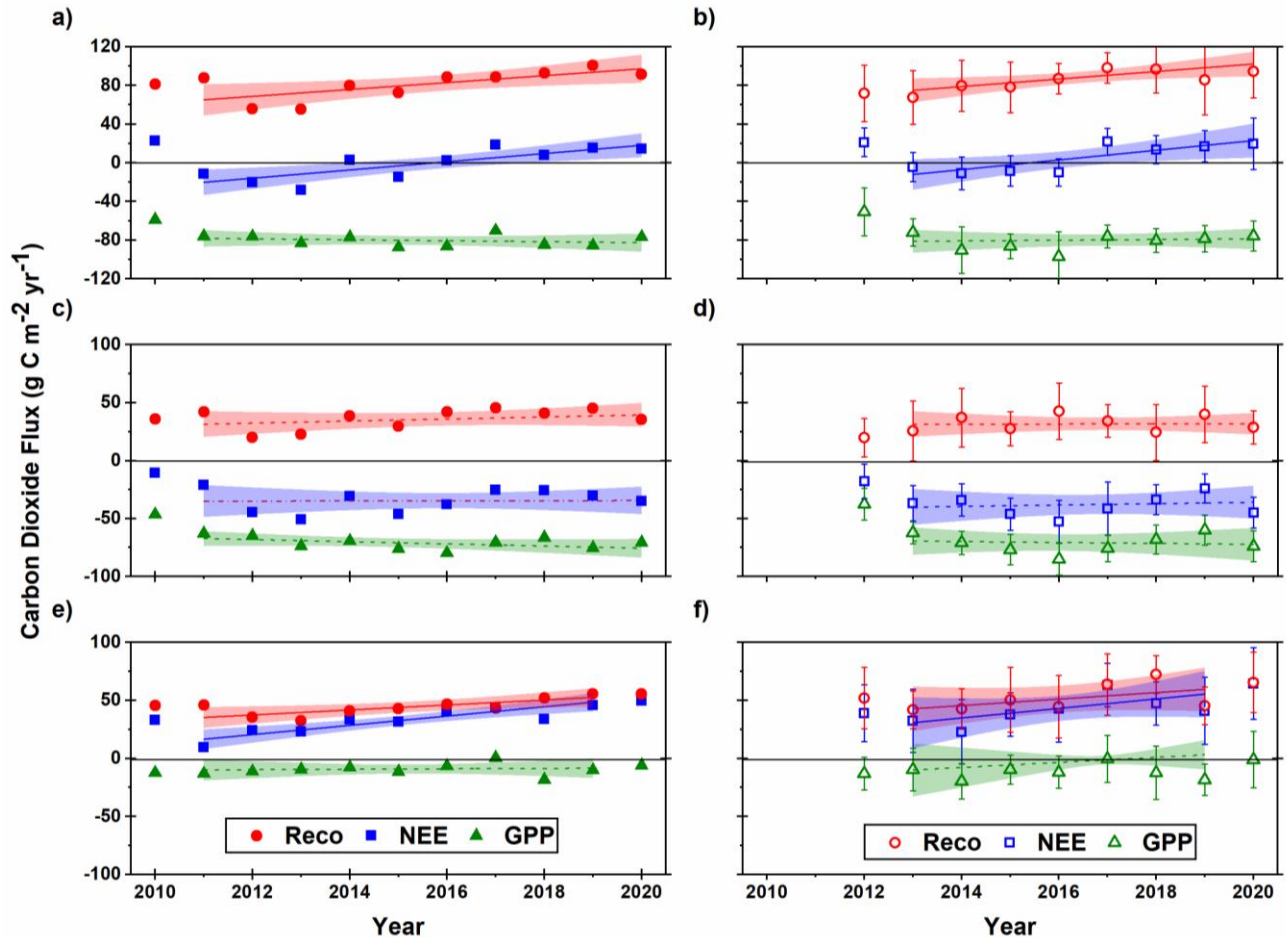
358 (0.18°C and 0.13°C over 10 years, respectively), whereas the growing season showed no  
359 significant change (0.1°C per 10 years;  $P = 0.053$ ).

360 From 2010 to 2020, the mean annual precipitation (snowfall and rainfall) was 395 mm, which  
361 ranging from 276 mm in 2014 to 385 mm in 2019, and was higher than the long-term average  
362 (377 mm,  $P = 0.05$ ). The relative length of the growing and non-growing seasons (2010-2020)  
363 was not significantly different from that of the long-term average, but the sum snowfall and total  
364 numbers of days with snow cover increased significantly from 2010 to 2020 (Supplementary Fig.  
365 S2) and were also higher than the long-term average ( $53.6 \pm 18.3$  vs  $30.9 \pm 16.3$  cm for sum  
366 snowfall and  $41.0 \pm 15.0$  vs  $18.0 \pm 11.0$  days for snow cover time, respectively; Table 1). The  
367 mean annual soil temperature for 0-30 cm was  $-0.8^{\circ}\text{C}$  in the period 2010-2020, higher than the  
368 long-term average of  $-1.2^{\circ}\text{C}$ . The mean soil water content for 0-30 cm during the growing  
369 season was 11.3% from 2010 to 2020, which was not significantly different from the long-term  
370 average (10.8%). The mean active layer thickness (ALT) on Beilu'He was  $185 \pm 17$  cm and  
371 significantly increased by a rate of  $3.5 \text{ cm yr}^{-1}$  in the period 2010-2020, resulting in a  
372 considerably deeper ALT than the long-term average (mean ALT was  $132.0 \pm 38.0$  cm).

373 **Table 1.** Environmental variables measured at the site during growing season (Grow. Seas.), non-growing season (N-Grow. Seas.) and  
 374 the reference period between 1<sup>st</sup> March and 15<sup>th</sup> June used as a proxy for the high carbon dioxide emissions at the end of the non-  
 375 growing season and at the start of the growing season. The values are reported for the decade 2010-2020 and the long-term 1975-2020.

Environmental Variables	2010-2020			Long-term (1975-2020)		
	Grow. Seas.	N-Grow. Seas.	1 <sup>st</sup> March to 15 <sup>th</sup> June	Grow. Seas.	N-Grow. Seas.	1 <sup>st</sup> March to 15 <sup>th</sup> June
Tair (°C)	4.0 ± 3.2	-8.9 ± 2.9	-3.5 ± 3.3	3.9 ± 1.6	-10.2 ± 5.1	-3.7 ± 2.2
Rainfall (mm)	35.0 ± 26.0	23.0 ± 14.0	67.0 ± 18.0	316.0 ± 20.0	21.0 ± 11.0	40.0 ± 16.0
Wind Speed (m s <sup>-1</sup> )	3.5 ± 2.7	5.1 ± 1.9	4.6 ± 1.8	3.3 ± 2.7	4.6 ± 4.1	4.2 ± 3.8
Tsoil (°C)	4.3 ± 3.0	-4.4 ± 3.8	-2.3 ± 2.9	3.7 ± 3.2	-4.6 ± 3.6	-2.5 ± 2.1
SWC (%)	14.4 ± 1.8	-	11.6 ± 2.0	15.0 ± 2.7	-	9.2 ± 7.3
TSF (cm)	7.7 ± 3.4	65.5 ± 12.4	53.6 ± 18.3	6.5 ± 5.9	35.1 ± 22.6	30.9 ± 16.3
SCD (d)	11.0 ± 10.0	47.0 ± 16.0	39.0 ± 15.0	13.0 ± 11.0	24.0 ± 13.0	18.0 ± 11.0
ALT (cm)	185.0 ± 17.0	-	36.0	132.0 ± 38.0	-	32.0

376 *Note.* Tair: air temperature at 3 m (°C); Rainfall: mm. The non-growing season rainfall does not include snow because the rainfall was  
 377 measured by a rain gauge only. Data for the total snowfall and snow cover days were obtained from the Wudao-Liang meteorology  
 378 service station, located 52 km away from the EC tower; Tsoil: soil temperature at 0-30 cm (°C); SWC: soil water content at 0-30 cm  
 379 (%); TSF: total snowfall (cm); SCD: snow cover days (d); ALT: the thickness of the active layer (cm); Grow. Seas.: growing season,  
 380 from 1<sup>st</sup> May to 30<sup>th</sup> September; N-Grow. Seas.: non-growing season, from 1<sup>st</sup> October to the next 30<sup>th</sup> April. Data presented are given  
 381 as means ± SD.



### 382 3.2 Temporal dynamics of ecosystem carbon dioxide flux

383 **Figure 1.** Time series of carbon dioxide (CO<sub>2</sub>) flux from an alpine steppe in Beilu'He, northwest  
 384 Tibetan Plateau using eddy-covariance (left column, solid symbols) and chamber-based (right  
 385 column, open symbols) approaches. a and b: annual total of CO<sub>2</sub> fluxes, c and d: CO<sub>2</sub> fluxes for  
 386 the growing season, e and f: fluxes for non-growing season. NEE: net ecosystem exchange (NEE,  
 387 g C m<sup>-2</sup> yr<sup>-1</sup>); R<sub>eco</sub>: ecosystem respiration (g C m<sup>-2</sup> yr<sup>-1</sup>); GPP: gross primary production (g C m<sup>-2</sup>  
 388 yr<sup>-1</sup>). The linear regression of annual total and growing season fluxes was based on the period  
 389 2011-2020, as we only had the July measurement for 2010. For fluxes from the non-growing  
 390 season, the linear regression was based on 2011-2019, because we lacked complete  
 391 measurements for 2010 and 2020. Solid lines are used to mark significant ( $p < 0.05$ ) changes,  
 392 whereas dashed lines indicate non-significant changes ( $p > 0.05$ ). Shading illustrates the 95%  
 393 confidence intervals.

394  
395  
396 During 2011-2020, the mean annual ecosystem carbon exchange (NEE) rate measured by EC  
397 was  $1.4 \pm 15.5 \text{ g C m}^{-2} \text{ yr}^{-1}$  (ranging from  $-28.1 \pm 20.0 \text{ g C m}^{-2} \text{ yr}^{-1}$  of 2012 to  $18.6 \pm 17.59 \text{ g C}$   
398  $\text{m}^{-2} \text{ yr}^{-1}$  of 2017), lower than the value of  $4.9 \pm 13.5 \text{ g C m}^{-2} \text{ yr}^{-1}$  which was measured by the  
399 automatic chamber for the period 2013-2020 (ranging from  $-10.8 \pm 17.0 \text{ g C m}^{-2} \text{ yr}^{-1}$  for 2014 to  
400  $21.9 \pm 13.8 \text{ g C m}^{-2} \text{ yr}^{-1}$  for 2017) (Figs. 1a and b). The ANOVA results indicate that the NEE  
401 rates measured by both EC and the automatic chamber significantly increased during the study  
402 period ( $p < 0.01$ ). During the growing season (1<sup>st</sup> May to 30<sup>th</sup> September), the ecosystem was a  
403 consistent CO<sub>2</sub> sink, while for the non-growing season (1<sup>st</sup> October to 30<sup>th</sup> April), the ecosystem  
404 was a consistent CO<sub>2</sub> source over the entire study period. Specifically, the mean NEE rates of the  
405 growing season were  $-34.7 \pm 11.4 \text{ g C m}^{-2} \text{ yr}^{-1}$  (ranging from  $-50.9 \pm 14.8$  in 2013 to  $-21.0 \pm$   
406  $24.6 \text{ g C m}^{-2} \text{ yr}^{-1}$  in 2011) and  $-39.2 \pm 8.4 \text{ g C m}^{-2} \text{ yr}^{-1}$  (ranging from  $-52.5 \pm 18.5 \text{ g C m}^{-2} \text{ yr}^{-1}$   
407 in 2016 to  $-23.9 \pm 12.7 \text{ g C m}^{-2} \text{ yr}^{-1}$  in 2019), measured by EC and the automatic chamber,  
408 respectively. For the non-growing season, the mean NEE rate measured by EC was  $33.3 \pm 6.9 \text{ g}$   
409  $\text{C m}^{-2} \text{ yr}^{-1}$ , with a clear increase of about fivefold from  $9.3 \pm 17.6 \text{ g C m}^{-2} \text{ yr}^{-1}$  of 2011 to  $49.5 \pm$   
410  $26.5 \text{ g C m}^{-2} \text{ yr}^{-1}$  of 2020.

411 Surprisingly, several high CO<sub>2</sub> emission events were noted at the end of the non-growing season  
412 and at the start of the growing season, which covered 1<sup>st</sup> March to 15<sup>th</sup> June (Fig. 2). From 2011  
413 to 2020, the mean CO<sub>2</sub> emission rate of this period was  $15.4 \text{ g C m}^{-2} \text{ yr}^{-1}$ , ranging from  $14.6 \pm$   
414  $10.7 \text{ g C m}^{-2} \text{ yr}^{-1}$  in 2012 to  $35.3 \pm 12.1 \text{ g C m}^{-2} \text{ yr}^{-1}$  in 2017. Emissions significantly increased  
415 over the period 2011-2020, with an average rate of  $22.6 \text{ g C m}^{-2} \text{ decade}^{-1}$  (Supplementary Fig.  
416 S3), which accounted for annual emissions of 23.2% and 25.8%, respectively.

417 Fig. 1 indicates that the mean annual R<sub>eco</sub> based on EC was  $81.3 \pm 14.1 \text{ g C m}^{-2} \text{ yr}^{-1}$ , slightly

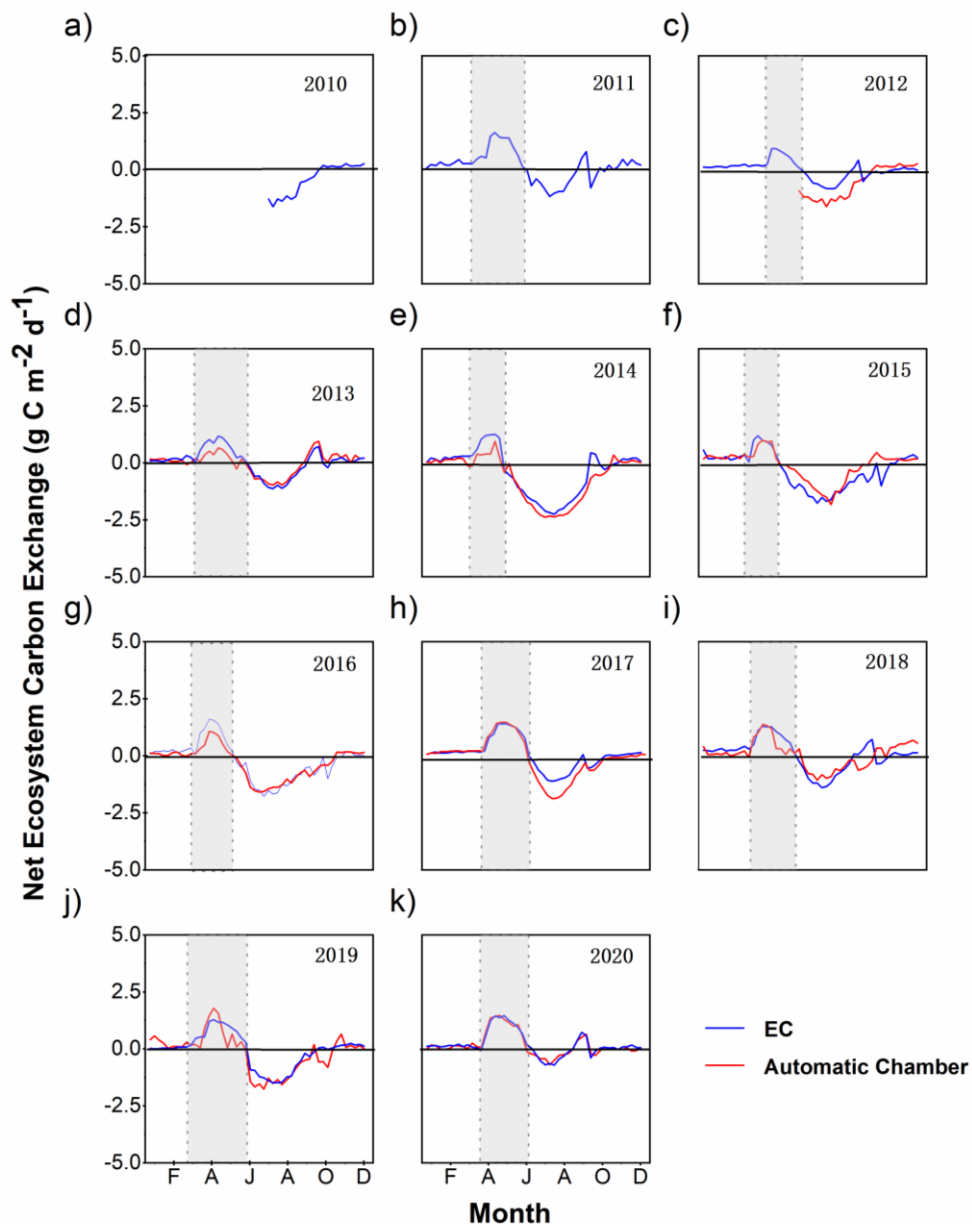
418 lower than that measured by the automatic chamber ( $84.3 \pm 10.3 \text{ g C m}^{-2} \text{ yr}^{-1}$ ). The highest  
419 annual  $R_{\text{eco}}$  was found in 2019 for EC, whereas it occurred in 2017 for the automatic chamber  
420 method. In addition, the minimum values of  $R_{\text{eco}}$  occurred in 2013 for both the EC and automatic  
421 chamber measurements.

422 From 2011 to 2020, the annual EC-measured  $R_{\text{eco}}$  showed a significant increase at a rate of  $26.3$   
423  $\text{g C m}^{-2} \text{ decade}^{-1}$ , ranging from  $55.2 \pm 13.8 \text{ g C m}^{-2} \text{ yr}^{-1}$  to  $100.8 \pm 12.6 \text{ g C m}^{-2} \text{ yr}^{-1}$  (the  
424 automatic chamber increased at a rate of  $32.9 \text{ g C m}^{-2} \text{ decade}^{-1}$ , ranging from  $67.5 \pm 27.6 \text{ g C}$   
425  $\text{m}^{-2} \text{ yr}^{-1}$  to  $98.0 \pm 15.6 \text{ g C m}^{-2} \text{ yr}^{-1}$ ). During the growing season, the mean  $R_{\text{eco}}$  was  $36.2 \pm 8.2 \text{ g}$   
426  $\text{C m}^{-2} \text{ yr}^{-1}$  with EC, which is very similar to the automatic chamber measurement ( $31.1 \pm 7.3 \text{ g C}$   
427  $\text{m}^{-2} \text{ yr}^{-1}$ ). There were no significant changes in the  $R_{\text{eco}}$  of the growing period in both the EC and  
428 automatic chamber measurements. For the non-growing season,  $R_{\text{eco}}$  accounted for more than  
429 half of the total annual  $R_{\text{eco}}$  (55.9% for EC and 62.9% for the automatic chamber).

430 The mean annual GPP was  $-78.4 \pm 8.1 \text{ g C m}^{-2} \text{ yr}^{-1}$  for both the EC and automatic chamber and  
431 showed no significant interannual variability ( $p > 0.05$ ; Fig. 1). The growing season accounted  
432 for 87.6% and 86.1 of the annual GPP for the EC and automatic chamber measurements,  
433 respectively. The non-growing season contributed relatively little to the annual GPP ( $-18.4 \pm$   
434  $12.4$  to  $-0.4 \pm 20.7 \text{ g C m}^{-2} \text{ yr}^{-1}$  for the EC and automatic chamber measurements, respectively)  
435 and no significant change was found over time with either method.

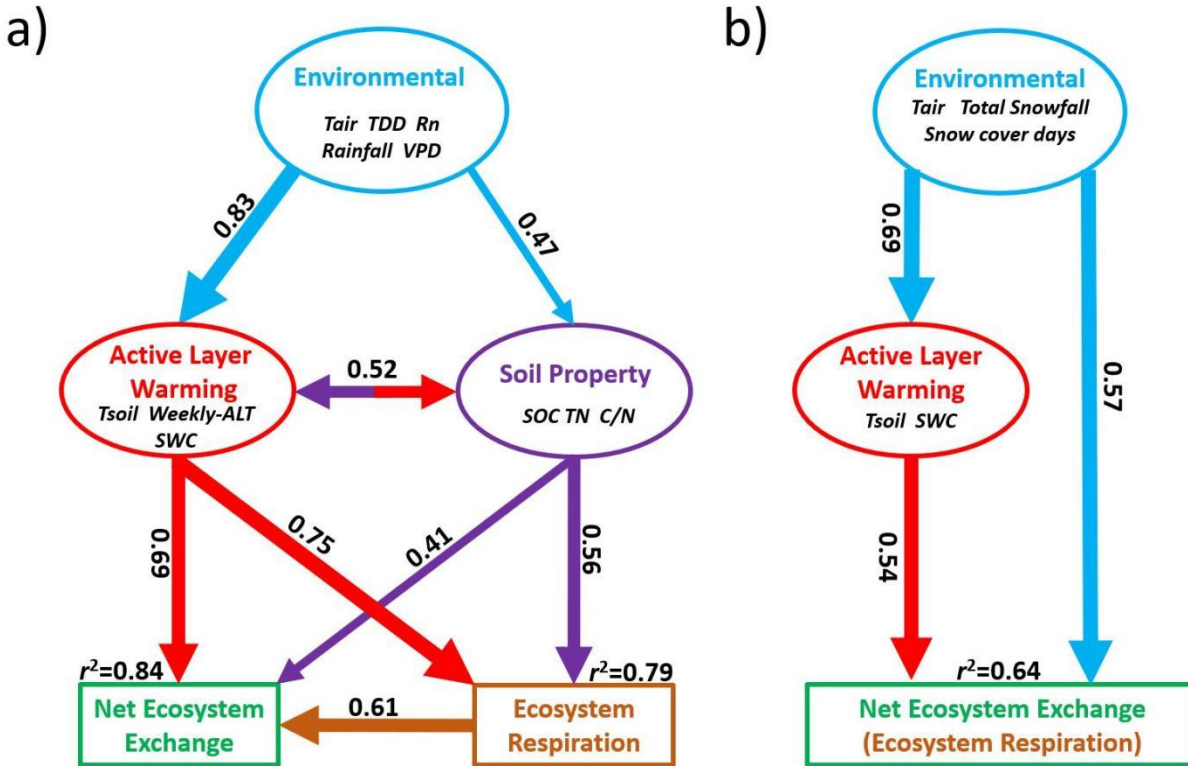
436

437  
 438 **Fig**  
 439 **ure**  
 440 **2.**  
 441 Dai  
 442 ly  
 443 net  
 444 eco  
 445 syst  
 446 em  
 447 exc  
 448 han  
 449 ge  
 450 (N  
 451 EE,  
 452 g C  
 453 m<sup>-2</sup>  
 454 d<sup>-1</sup>)  
 455 me  
 456 asu  
 457 red  
 458 by  
 459 the  
 460 edd



461 y covariance (EC, blue line) and automatic chamber (red line). Grey-shaded areas depict the  
 462 period with high carbon dioxide (CO<sub>2</sub>) emissions from the end of the non-growing season to the  
 463 early growing season. The start and end time of the CO<sub>2</sub> flux high emission events are marked as  
 464 grey dotted lines. Here, if the CO<sub>2</sub> emission was 5 times the mean CO<sub>2</sub> flux of winter for 3  
 465 successive days, it was defined as the start day of the ‘high emission period’. When the CO<sub>2</sub>  
 466 emission was equal to the mean CO<sub>2</sub> flux of winter for 3 successive days, it was defined as the  
 467 end day of the ‘high emission period’.





468 **3.3 Drivers of carbon dioxide flux**

469 **Figure 3.** Structural equation modelling (SEM) with considered variables (in coloured ellipses)  
 470 and potential relationships (arrows) for net ecosystem exchange (NEE, green box) over (a) the  
 471 growing season and (b) the non-growing season using data from EC and the automatic chamber.  
 472 The double-headed arrows represent the covariance between the two variables. The single-  
 473 headed arrows indicate the direction of the linkage. The arrow width is proportional to the  
 474 strength of the path coefficients. The numbers are standardized path coefficients, which reflect  
 475 the importance of the variables within the model (Colman & Schimel, 2013). ‘Environmental’  
 476 includes air temperature at 3 m ( $T_{air}$ ), thawing degree days (TDD), net radiation (Rn), rainfall,  
 477 vapour pressure deficit (VPD), total snowfall and snow cover days. ‘Active layer warming’  
 478 includes soil temperature of 0-30 cm ( $T_{soil}$ ), weekly active layer depth (weekly; ALT) and soil  
 479 water content of 0-30 cm (SWC); ‘soil property’ for 0-30 cm depth includes soil organic carbon  
 480 (SOC), pH and total nitrogen (TN) and the ratio of SOC to TN concentrations (C/N). The model  
 481 for the growing season had  $\chi^2 = 6.83$  and RMSEA = 0.08, whereas the model for the non-

482 growing season had  $\chi^2 = 7.08$  and RMSEA = 0.09.

483 The Structure equation modelling (SEM) illustrates the direct and indirect links between net  
484 ecosystem exchange (NEE), environmental variables and the thickness of the active layer, soil  
485 temperatures of 0-30 cm and soil water content of 0-30 cm (Fig. 3). Here, important drivers of  
486 NEE in the growing season were identified: active layer warming and soil properties. The SEM  
487 model suggests that the active layer warming and soil properties could explain 78% of the NEE  
488 variations during the growing season and that active layer warming alone could explain 64% of  
489 the NEE in the non-growing season (Fig. 3).

490

## 491 **4. Discussion**

### 492 **4.1 Ecosystem carbon budget for the alpine steppe ecosystem on the Tibetan Plateau**

493 Ten years of year-round carbon dioxide (CO<sub>2</sub>) flux measurements in the alpine steppe ecosystem  
494 of the Beilu'He region on the Tibetan Plateau show that the site has switched from being a net  
495 annual sink (or close to neutral) of CO<sub>2</sub> to a net source of CO<sub>2</sub> to the atmosphere (the shift was  
496 from  $-28.1 \pm 20.0$  to  $21.9 \pm 13.8$  g C m<sup>-2</sup> yr<sup>-1</sup>). The study site is dominated by the following plant  
497 species: *C. moorcroftii* Falc. ex Boott, *K. tibetica* Maxim, *A. tanggulashanensis* and *R. tibetica*,  
498 which represent an ecosystem type covering approximately 34% of the permafrost region on the  
499 Tibetan Plateau (the Tibetan Plateau area is  $250 \times 10^4$  km<sup>2</sup> according to Ding et al. (2016)). Based  
500 on the 4.5 °C IPCC representative concentration pathway, this type of ecosystem will account for  
501 76% of the Tibetan Plateau in 2100 (Zhang et al., 2015).

502 Long-term flux measurements carried out in this type of ecosystem are rare (Li et al., 2015; Yun  
503 et al., 2018). Most of the reported Tibetan Plateau CO<sub>2</sub> flux data have been collected for wet

504 tundra ecosystems (Zhang et al., 2018; Liu et al., 2019) or seasonal permafrost regions (Li et al.,  
505 2016; Niu et al., 2017), in which larger annual rates for GPP and  $R_{\text{eco}}$  were observed. In this  
506 study, annual NEE measurements from both EC and automatic chambers ( $-1.4 \pm 15.5$  vs  $4.9 \pm$   
507  $13.5 \text{ g C m}^{-2} \text{ yr}^{-1}$ , respectively) were within the range of the results of other studies conducted on  
508 the Tibetan Plateau or in Arctic tundra upland ecosystems (Trucco et al., 2012; Li et al., 2016;  
509 Kim et al., 2016; Zhang et al., 2018).

510

#### 511 **4.2 Interannual and seasonal variations of carbon dioxide fluxes**

512 The trends for interannual variations of the year-round NEE estimated using both EC and  
513 automatic chamber measurements revealed that the studied alpine steppe ecosystem has been in  
514 transition from being a net  $\text{CO}_2$  sink to a net  $\text{CO}_2$  source since 2010. This transition has primarily  
515 been driven by increasing ecosystem respiration and a corresponding increase in  $\text{CO}_2$  emissions  
516 during the non-growing season. Our results are in line with a previous meta-data analysis study  
517 by McGuire et al. (2012) and Belshe et al. (2013), which suggested that annual  $\text{CO}_2$  emissions  
518 could exceed  $\text{CO}_2$  uptake across the tundra biome, based on 40 years of  $\text{CO}_2$  flux data across 32  
519 sites at high latitudes. Our findings also agree with a more recent synthesis study by Natali et al.  
520 (2019), based on both process-based models and non-growing season (October-April)  $\text{CO}_2$  flux  
521 observations across the Pan-Arctic region, which indicates that enhanced soil  $\text{CO}_2$  loss as a result  
522 of winter warming may offset growing season carbon uptake in the future.

523 The seasonal pattern of  $\text{CO}_2$  fluxes is characterized by considerable  $\text{CO}_2$  emissions from the end  
524 of the non-growing season to the early growing season (from 1<sup>st</sup> March to 15<sup>th</sup> June; Fig. 2). The  
525 high  $\text{CO}_2$  emissions were significantly correlated with total snowfall, snow cover days and soil

526 water content at 0-30 cm (Supplementary Fig. 4). The start time of high CO<sub>2</sub> emissions was close  
527 to the first snow melt event in March (data not shown). The large CO<sub>2</sub> fluxes can be explained by  
528 at least two sets of processes: one process related to CO<sub>2</sub> production during winter and trapped  
529 CO<sub>2</sub> within the pore space of soils during winter and released upon soil thawing (Elberling &  
530 Brandt, 2003; Raz-Yaseef et al., 2017). The second set of processes is related to potential  
531 accelerated microbial activities as well as increased availability of labile C in soils (Pirk et al.,  
532 2017). Therefore, the recovery of microbial activity synchronous with the increasing substrate  
533 availability could be partly responsible for the relatively large CO<sub>2</sub> emissions (bursts) at the end  
534 of the non-growing season and in the early part of the growing season (Liu et al., 2020). Future  
535 work is needed to differentiate these two explanations for the Tibetan Plateau study site.

536

### 537 **4.3 Key driver of the variation of seasonal carbon dioxide fluxes**

538 In this study, active layer warming was identified as one of the key drivers controlling NEE  
539 throughout both the growing and non-growing seasons, which is consistent with the findings of  
540 research conducted in Arctic regions (Trucco et al., 2012; Gerardo et al., 2017; Rodenhizer et al.,  
541 2020). Increased NEE as a result of active layer warming is associated with increased nutrient  
542 availability for both plants and microorganism communities (Pries et al., 2015) and increased  
543 accessibility for microbes to deeper located labile soil carbon pools (Schuur et al., 2007;  
544 Elberling et al., 2010; Koven et al., 2015). It is beyond the scope of this study to quantify  
545 whether thawing permafrost has directly influenced the increased CO<sub>2</sub> production. But we  
546 conclude that warming and accelerated near-surface SOC turnover alone can explain the  
547 observed shift of the ecosystem from being a sink to a source over the studied 10-year period.

548 From 2010 to 2020, GPP of the growing season as well as the non-growing season showed no  
549 significant increase in response to temperature rise, which contrasts with the findings for the  
550 Arctic dry tundra that GPP has a higher temperature sensitivity based on open top chamber  
551 measurements (Welker et al., 2004) and EC monitors (Ueyama et al., 2014). This suggests that  
552 GPP can be affected by changes in vegetation properties, e.g., the leaf area index, stomatal  
553 conductance (Schädel et al., 2018; Grant et al., 2019; Chen et al., 2021) and other drivers of  
554 photosynthesis, e.g., air temperature, net solar radiation, soil water content and even the leaf C/N  
555 ratio (Oechel et al., 2014; Webb et al., 2016; Celis et al., 2017). On the Tibetan Plateau, 40 years  
556 of monitoring data indicates that significant changes in air temperature and precipitation took  
557 place mainly during winter (Yao et al., 2018). Fig. 1 suggests that neither the NEE, GPP nor  $R_{eco}$   
558 changed significantly during the growing season over the study period. However, the interannual  
559 variations in NEE and  $R_{eco}$  and the observations during the non-growing season showed a  
560 significant increase, which was mainly explained by the increasing active layer warming over  
561 time. The response of increased air temperature during the non-growing season on GPP may  
562 however not be representative of other ecosystem types depending on the site-specific  
563 hydrological conditions (Welker et al., 2004).

564 Interestingly, during the growing season, the soil temperature (5.9 °C) and soil water content  
565 (15%) measured at a 0-30cm depth interval were comparable to those observed in Arctic heath  
566 sites (soil temperature was 5.6°C and soil water content was 14.5% for 0-30 cm depth; Lund et al.  
567 (2012)). However, the mean daily NEE of alpine steppe on the Tibetan Plateau was  $-1.2 \text{ g C m}^{-2}$   
568  $\text{d}^{-1}$ , as compared to  $-0.7$  to  $-0.6 \text{ g C m}^{-2} \text{ d}^{-1}$  at the Arctic heath site. In contrast, NEE measured in  
569 this study with EC was almost equal to the NEE measured in a high Arctic semi-desert site on  
570 Svalbard ( $-1.3 \text{ g C m}^{-2} \text{ d}^{-1}$ , measured from 31<sup>st</sup> July to 11<sup>st</sup> August; Lüers et al. (2014)), with a

571 soil temperature at 0-50 cm depth interval of 6.1°C and SWC < 7%. This suggests that soil  
572 temperature and SWC may greatly influence the carbon cycle in permafrost-affected ecosystems,  
573 but also that regions may differ in terms of carbon sink and source activities despite similarities  
574 in the presence of permafrost or short growing seasons. Other environmental factors may control  
575 the overall carbon sink/source capacity, such as ALT (Peries et al., 2017), water table depth  
576 (Celis et al., 2020), even net radiation (Shen et al., 2015), or soil physical factors, e.g., the  
577 aggregate protection (Qin et al., 2019).

578

#### 579 **4.4 Uncertainties and limitations**

580 In this study, during the winter (November to January) the ground was frozen and plants were  
581 dormant, but a CO<sub>2</sub> uptake was still measurable and documented in data from both EC and the  
582 automatic chamber (data not shown) at noon time and low wind speed (< 2 m s<sup>-1</sup>) conditions. It  
583 remains unclear what might cause this uptake in winter. Some studies (e.g., Semikhatova et al.,  
584 2009; Starr & Oberbauer, 2003) have linked CO<sub>2</sub> uptake in the non-growing season with the  
585 photosynthetic activities of evergreen plants and soil crust plants (Starr & Oberbauer, 2003). In  
586 this study, we have taken a conservative approach and consider the CO<sub>2</sub> uptake in winter to be  
587 negligible. This means there might be slight overestimations of winter CO<sub>2</sub> release.

588

#### 589 **5. Conclusions**

590 This study summarizes measured CO<sub>2</sub> fluxes in a high alpine steppe site on the northwest  
591 Tibetan Plateau (Beilu'He) for the period 2010-2020 using eddy covariance and automatic  
592 chamber approaches. During 2010-2020, the study site switched from being a net annual sink of

593 CO<sub>2</sub> or neutral to a net source of CO<sub>2</sub> to the atmosphere. The structural equation model analysis  
594 revealed that active layer warming and soil properties were the most important direct drivers of  
595 variations in R<sub>eco</sub> during the growing season (2010-2020). It also showed that active layer  
596 warming was the major driver of the R<sub>eco</sub> changes in the non-growing season linked to changes  
597 in snow cover. GPP showed no significant trend corresponding to the warming (mainly during  
598 winter), which could be due to a lack of sufficient nutrients despite a warmer climate. Overall,  
599 these results imply that changes in NEE reflect several interacting processes regulated by both  
600 direct and indirect controls on active layer warming and soil properties. Our hypotheses will now  
601 be addressed in turn as follows: (1) ecosystem respiration has increased significantly due to  
602 increasing temperatures; mainly during the non-growing season; (2) increased precipitation has  
603 not resulted in major changes but has reduced the annual GPP due to a shorter growing season  
604 and potential loss of plant-available nutrients; and (3) despite warmer and wetter conditions,  
605 increases in plant growth were limited and no changes in GPP were noted during the study  
606 period. Thus, this study reveals that the study site and possibly around a third of the Tibetan dry  
607 grassland have now switched from being a sink into a source of CO<sub>2</sub> to the atmosphere.

608

## 609 **References**

- 610 Asparouhov, T., Hamaker, E. L., & Muthén, B. (2018). Dynamic structural equation  
611 models. *Structural Equation Modeling: A Multidisciplinary Journal*, 25(3), 359-388.  
612 <https://doi.org/10.1080/10705511.2017.1406803>
- 613 Aubinet, M., Grelle, A., Ibrom, A., Rannik, Ü., Moncrieff, J., Foken, T., et al. (1999). Estimates  
614 of the annual net carbon and water exchange of forests: the EUROFLUX  
615 methodology. *Advances in Ecological Research*, 30, 113-175.

616 [https://doi.org/10.1016/S0065-2504\(08\)60018-5](https://doi.org/10.1016/S0065-2504(08)60018-5)

617 Belshe, E. F., Schuur, E. A. G., & Bolker, B. M. (2013). Tundra ecosystems observed to be CO<sub>2</sub>  
618 sources due to differential amplification of the carbon cycle. *Ecology Letters*, 16(10),  
619 1307-1315.  
620 <https://doi.org/10.1111/ele.12164>

621 Belshe, E. F., Schuur, E. A. G., Bolker, B. M., & Bracho, R. (2012). Incorporating spatial  
622 heterogeneity created by permafrost thaw into a landscape carbon estimate. *Journal of*  
623 *Geophysical Research: Biogeosciences*, 117(G1).  
624 <https://doi.org/10.1029/2011JG001836>

625 Burba, G. G., McDERMITT, D. K., Grelle, A. anderson, D. J., & Xu, L. (2008). Addressing the  
626 influence of instrument surface heat exchange on the measurements of CO<sub>2</sub> flux from  
627 open-path gas analyzers. *Global Change Biology*, 14(8), 1854-1876.  
628 <https://doi.org/10.1111/j.1365-2486.2008.01606.x>

629 Celis, G., Mauritz, M., Bracho, R., Salmon, V. G., Webb, E. E., Hutchings, J., et al. (2017).  
630 Tundra is a consistent source of CO<sub>2</sub> at a site with progressive permafrost thaw during 6  
631 years of chamber and eddy covariance measurements. *Journal of Geophysical Research:*  
632 *Biogeosciences*, 122(6), 1471-1485.  
633 <https://doi.org/10.1002/2016JG003671>

634 Chen, A., Mao, J., Ricciuto, D., Xiao, J., Frankenberg, C., Li, X., & Knapp, A. K. (2021).  
635 Moisture availability mediates the relationship between terrestrial gross primary  
636 production and solar-induced chlorophyll fluorescence: Insights from global-scale  
637 variations. *Global change biology*, 27(6), 1144-1156.  
638 <https://doi.org/10.1111/gcb.15373>

639 Chen, D., Xu, B., Yao, T., Guo, Z., Cui, P., Chen, F., et al. (2015). Assessment of past, present  
640 and future environmental changes on the Tibetan Plateau. *Chinese Science*  
641 *Bulletin*, 60(32), 3025-3035.  
642 <https://doi.org/10.1360/N972014-01370>

643 Chen, L., Liang, J., Qin, S., Liu, L. I., Fang, K., Xu, Y., ... & Yang, Y. (2016). Determinants of  
644 carbon release from the active layer and permafrost deposits on the Tibetan  
645 Plateau. *Nature Communications*, 7(1), 1-12.  
646 <https://doi.org/10.1038/ncomms13046>



647 Cheng, G., Zhao, L., Li, R., Wu, X., Sheng, Y., Hu, G., et al. (2019). Characteristic, changes and  
648 impacts of permafrost on Qinghai-Tibet Plateau. *Chinese Science Bulletin*, 64(27), 2783-  
649 2795.  
650 <https://doi.org/10.1360/TB-2019-0191>

651 Colman, B. P., & Schimel, J. P. (2013). Drivers of microbial respiration and net N mineralization  
652 at the continental scale. *Soil Biology and Biochemistry*, 60, 65-76.  
653 <https://doi.org/10.1016/j.soilbio.2013.01.003>

654 Corradi, C., Kolle, O., Walter, K., Zimov, S. A., & Schulze, E. D. (2005). Carbon dioxide and  
655 methane exchange of a north-east Siberian tussock tundra. *Global Change  
656 Biology*, 11(11), 1910-1925.  
657 <https://doi.org/10.1111/j.1365-2486.2005.01023.x>

658 Davidson, E. A., & Janssens, I. A. (2006). Temperature sensitivity of soil carbon decomposition  
659 and feedbacks to climate change. *Nature*, 440(7081), 165-173.  
660 <https://doi.org/10.1038/nature04514>

661 Ding, J., Li, F., Yang, G., Chen, L., Zhang, B., Liu, L., et al. (2016). The permafrost carbon  
662 inventory on the Tibetan Plateau: a new evaluation using deep sediment cores. *Global  
663 Change Biology*, 22(8), 2688-2701.  
664 <https://doi.org/10.1111/gcb.13257>

665 Ding, J., Chen, L., Ji, C., Hugelius, G., Li, Y., Liu, L., ... & Yang, Y. (2017). Decadal soil carbon  
666 accumulation across Tibetan permafrost regions. *Nature Geoscience*, 10(6), 420-424.  
667 <https://doi.org/10.1038/ngeo2945>

668 Elberling, B., & Brandt, K. K. (2003). Uncoupling of microbial CO<sub>2</sub> production and release in  
669 frozen soil and its implications for field studies of arctic C cycling. *Soil Biology and  
670 Biochemistry*, 35(2), 263-272.  
671 [https://doi.org/10.1016/S0038-0717\(02\)00258-4](https://doi.org/10.1016/S0038-0717(02)00258-4)

672 Elberling, B., Michelsen, A., Schädel, C., Schuur, E. A., Christiansen, H. H., Berg, L., et al.  
673 (2013). Long-term CO<sub>2</sub> production following permafrost thaw. *Nature Climate  
674 Change*, 3(10), 890-894.  
675 <https://doi.org/10.1038/nclimate1955>

676 Elberling, B., Christiansen, H. H., & Hansen, B. U. (2010). High nitrous oxide production from  
677 thawing permafrost. *Nature Geoscience*, 3(5), 332-335.

678 <https://doi.org/10.1038/ngeo803>

679 Epstein, H. E., Myers-Smith, I., & Walker, D. A. (2013). Recent dynamics of arctic and sub-  
680 arctic vegetation. *Environmental Research Letters*, 8(1), 015040.

681 <https://doi.org/10.1088/1748-9326/8/1/015040>

682 Euskirchen, E. S., Bret-Harte, M. S., Shaver, G. R., Edgar, C. W., & Romanovsky, V. E. (2017).  
683 Long-term release of carbon dioxide from arctic tundra ecosystems in  
684 Alaska. *Ecosystems*, 20(5), 960-974.

685 <https://doi.org/10.1007/s10021-016-0085-9>

686 Fox, A. M., Huntley, B., Lloyd, C. R., Williams, M., & Baxter, R. (2008). Net ecosystem  
687 exchange over heterogeneous Arctic tundra: Scaling between chamber and eddy  
688 covariance measurements. *Global Biogeochemical Cycles*, 22(2).

689 <https://doi.org/10.1029/2007GB003027>

690 Goulden, M. L., Munger, J. W., Fan, S. M., Daube, B. C., & Wofsy, S. C. (1996). Measurements  
691 of carbon sequestration by long-term eddy covariance: Methods and a critical evaluation  
692 of accuracy. *Global Change Biology*, 2(3), 169-182.

693 <https://doi.org/10.1111/j.1365-2486.1996.tb00070.x>

694 Grant, R. F., Mekonnen, Z. A., & Riley, W. J. (2019). Modeling climate change impacts on an  
695 Arctic polygonal tundra: 1. Rates of permafrost thaw depend on changes in vegetation  
696 and drainage. *Journal of Geophysical Research: Biogeosciences*, 124(5), 1308-1322.

697 <https://doi.org/10.1029/2018JG004644>

698 Hicks Pries, C. E., van Logtestijn, R. S., Schuur, E. A., Natali, S. M., Cornelissen, J. H., Aerts,  
699 R., et al. (2015). Decadal warming causes a consistent and persistent shift from  
700 heterotrophic to autotrophic respiration in contrasting permafrost ecosystems. *Global*  
701 *Change Biology*, 21(12), 4508-4519.

702 <https://doi.org/10.1111/gcb.13032>

703 Hugelius, G., Bockheim, J. G., Camill, P., Elberling, B., Grosse, G., Harden, J. W., et al. (2013).  
704 A new data set for estimating organic carbon storage to 3 m depth in soils of the northern  
705 circumpolar permafrost region. *Earth System Science Data*, 5(2), 393-402.

706 <https://doi.org/10.5194/essd-5-393-2013>

707 Jin, H., Yu, Q., Lü, L., Guo, D., He, R., Yu, S., et al. (2007). Degradation of permafrost in the  
708 Xing'anling Mountains, Northeastern China. *Permafrost and Periglacial Processes*, 18(3),

709 245-258.  
710 <https://doi.org/10.1002/ppp.589>

711 Kljun, N., Calanca, P., Rotach, M. W., & Schmid, H. P. (2015). A simple two-dimensional  
712 parameterisation for Flux Footprint Prediction (FFP). *Geoscientific Model*  
713 *Development*, 8(11), 3695-3713.  
714 <https://doi.org/10.5194/gmd-8-3695-2015>

715 Koven, C. D., Lawrence, D. M., & Riley, W. J. (2015). Permafrost carbon- climate feedback is  
716 sensitive to deep soil carbon decomposability but not deep soil nitrogen  
717 dynamics. *Proceedings of the National Academy of Sciences*, 112(12), 3752-3757.  
718 <https://doi.org/10.1073/pnas.1415123112>

719 Li, H., Zhang, F., Li, Y., Wang, J., Zhang, L., Zhao, L., et al. (2016). Seasonal and inter-annual  
720 variations in CO<sub>2</sub> fluxes over 10 years in an alpine shrubland on the Qinghai-Tibetan  
721 Plateau, China. *Agricultural and Forest Meteorology*, 228, 95-103.  
722 <https://doi.org/10.1016/j.agrformet.2016.06.020>

723 Li, Y., Dong, S., Liu, S., Zhou, H., Gao, Q., Cao, G., et al. (2015). Seasonal changes of CO<sub>2</sub>,  
724 CH<sub>4</sub> and N<sub>2</sub>O fluxes in different types of alpine grassland in the Qinghai-Tibetan Plateau  
725 of China. *Soil Biology and Biochemistry*, 80, 306-314.  
726 <https://doi.org/10.1016/j.soilbio.2014.10.026>

727 Liu, F., Kou, D., Chen, Y., Xue, K., Ernakovich, J. G., Chen, L., et al. (2021). Altered microbial  
728 structure and function after thermokarst formation. *Global Change Biology*, 27(4), 823-  
729 835.  
730 <https://doi.org/10.1111/gcb.15438>

731 Liu, X., Zhu, D., Zhan, W., Chen, H., Zhu, Q., Hao, Y., et al. (2019). Five-year measurements of  
732 net ecosystem CO<sub>2</sub> exchange at a fen in the Zoige peatlands on the Qinghai-Tibetan  
733 Plateau. *Journal of Geophysical Research: Atmospheres*, 124(22), 11803-11818.  
734 <https://doi.org/10.1029/2019JD031429>

735 Lund, M., Falk, J. M., Friberg, T., Mbufong, H. N., Sigsgaard, C., Soegaard, H., et al. (2012).  
736 Trends in CO<sub>2</sub> exchange in a high Arctic tundra heath, 2000-2010. *Journal of*  
737 *Geophysical Research: Biogeosciences*, 117(G2).  
738 <https://doi.org/10.1029/2011JG001901>

739 Lupascu, M., Welker, J. M., Seibt, U., Maseyk, K., Xu, X., & Czimczik, C. I. (2014). High

740 Arctic wetting reduces permafrost carbon feedbacks to climate warming. *Nature Climate*  
741 *Change*, 4(1), 51-55.  
742 <https://doi.org/10.1038/nclimate2058>

743 Mauritz, M., Bracho, R., Celis, G., Hutchings, J., Natali, S. M., Pegoraro, E., et al. (2017).  
744 Nonlinear CO<sub>2</sub> flux response to 7 years of experimentally induced permafrost  
745 thaw. *Global Change Biology*, 23(9), 3646-3666.  
746 <https://doi.org/10.1111/gcb.13661>

747 McGuire, A. D., Christensen, T. R., Hayes, D., Heroult, A., Euskirchen, E., Kimball, J. S., et al.  
748 (2012). An assessment of the carbon balance of Arctic tundra: comparisons among  
749 observations, process models and atmospheric inversions. *Biogeosciences*, 9(8), 3185-  
750 3204.  
751 <https://doi.org/10.5194/bg-9-3185-2012>

752 Min, E., Wilcots, M. E., Naeem, S., Gough, L., McLaren, J. R., Rowe, R. J., et al. (2021).  
753 Herbivore absence can shift dry heath tundra from carbon source to sink during peak  
754 growing season. *Environmental Research Letters*, 16(2), 024027.  
755 <https://doi.org/10.1088/1748-9326/abd3d0>

756 Natali, S. M., Watts, J. D., Rogers, B. M., Potter, S., Ludwig, S. M., Selbmann, A. K., et al.  
757 (2019). Large loss of CO<sub>2</sub> in winter observed across the northern permafrost  
758 region. *Nature Climate Change*, 9(11), 852-857.  
759 <https://doi.org/10.1038/s41558-019-0592-8>

760 Niu, B., He, Y., Zhang, X., Du, M., Shi, P., Sun, W., et al. (2017). CO<sub>2</sub> exchange in an alpine  
761 swamp meadow on the central Tibetan plateau. *Wetlands*, 37(3), 525-543.  
762 <https://doi.org/10.1007/s13157-017-0888-2>

763 Niu, F., Gao, Z., Lin, Z., Luo, J., & Fan, X. (2019). Vegetation influence on the soil hydrological  
764 regime in permafrost regions of the Qinghai-Tibet Plateau, China. *Geoderma*, 354,  
765 113892.  
766 <https://doi.org/10.1016/j.geoderma.2019.113892>

767 Oechel, W. C., Vourlitis, G. L., Hastings, S. J., Zulueta, R. C., Hinzman, L., & Kane, D. (2000).  
768 Acclimation of ecosystem CO<sub>2</sub> exchange in the Alaskan Arctic in response to decadal  
769 climate warming. *Nature*, 406(6799), 978-981.  
770 <https://doi.org/10.1038/35023137>

771 Oechel, W. C., Laskowski, C. A., Burba, G., Gioli, B., & Kalhori, A. A. (2014). Annual patterns  
772 and budget of CO<sub>2</sub> flux in an Arctic tussock tundra ecosystem. *Journal of Geophysical*  
773 *Research: Biogeosciences*, 119(3), 323-339.  
774 <https://doi.org/10.1002/2013JG002431>

775 Piao, S., Zhang, X., Wang, T., Liang, E., Wang, S., Zhu, J., & Niu, B. (2019). Responses and  
776 feedback of the Tibetan Plateau's alpine ecosystem to climate change. *Chinese Science*  
777 *Bulletin*, 64(27), 2842-2855.  
778 <https://doi.org/10.1360/TB-2019-0074>

779 Pirk, N., Sievers, J., Mertes, J., Parmentier, F. J. W., Mastepanov, M., & Christensen, T. R.  
780 (2017). Spatial variability of CO<sub>2</sub> uptake in polygonal tundra: assessing low-frequency  
781 disturbances in eddy covariance flux estimates. *Biogeosciences*, 14(12), 3157-3169.  
782 <https://doi.org/10.5194/bg-14-3157-2017>

783 Plaza, C., Pegoraro, E., Bracho, R., Celis, G., Crummer, K. G., Hutchings, J. A., et al. (2019).  
784 Direct observation of permafrost degradation and rapid soil carbon loss in tundra. *Nature*  
785 *Geoscience*, 12(8), 627-631.  
786 <https://doi.org/10.1038/s41561-019-0387-6>

787 Qin, S., Chen, L., Fang, K., Zhang, Q., Wang, J., Liu, F., et al. (2019). Temperature sensitivity of  
788 SOM decomposition governed by aggregate protection and microbial  
789 communities. *Science Advances*, 5(7), eaau1218.  
790 <https://doi.org/10.1126/sciadv.aau1218>

791 Raz-Yaseef, N., Torn, M. S., Wu, Y., Billesbach, D. P., Liljedahl, A. K., Kneafsey, T. J., et al.  
792 (2017). Large CO<sub>2</sub> and CH<sub>4</sub> emissions from polygonal tundra during spring thaw in  
793 northern Alaska. *Geophysical Research Letters*, 44(1), 504-513.  
794 <https://doi.org/10.1002/2016GL071220>

795 Rodenhizer, H., Ledman, J., Mauritz, M., Natali, S. M., Pegoraro, E., Plaza, C., et al. (2020).  
796 Carbon thaw rate doubles when accounting for subsidence in a permafrost warming  
797 experiment. *Journal of Geophysical Research: Biogeosciences*, 125(6), e2019JG005528.  
798 <https://doi.org/10.1029/2019JG005528>

799 Schädel, C., Koven, C. D., Lawrence, D. M., Celis, G., Garnello, A. J., Hutchings, J., et al.  
800 (2018). Divergent patterns of experimental and model-derived permafrost ecosystem  
801 carbon dynamics in response to Arctic warming. *Environmental Research Letters*, 13(10),

802 105002.  
803 <https://doi.org/10.1088/1748-9326/aae0ff>

804 Schuur, E. A., McGuire, A. D., Schädel, C., Grosse, G., Harden, J. W., Hayes, D. J., et al. (2015).  
805 Climate change and the permafrost carbon feedback. *Nature*, 520(7546), 171-179.  
806 <https://doi.org/10.1038/nature14338>

807 Schuur, E. A., Crummer, K. G., Vogel, J. G., & Mack, M. C. (2007). Plant species composition  
808 and productivity following permafrost thaw and thermokarst in Alaskan  
809 tundra. *Ecosystems*, 10(2), 280-292.  
810 <https://doi.org/10.1007/s10021-007-9024-0>

811 Schuur, E. A., Vogel, J. G., Crummer, K. G., Lee, H., Sickman, J. O., & Osterkamp, T. E. (2009).  
812 The effect of permafrost thaw on old carbon release and net carbon exchange from  
813 tundra. *Nature*, 459(7246), 556-559.  
814 <https://doi.org/10.1038/nature08031>

815 Semikhatova, O. A., Ivanova, T. I., & Kirpichnikova, O. V. (2009). Respiration rate of arctic  
816 plants as related to the production process. *Russian Journal of Plant Physiology*, 56(3),  
817 306-315.  
818 <https://doi.org/10.1134/S1021443709030029>

819 Schuur, E. A., Bracho, R., Celis, G., Belshe, E. F., Ebert, C., Ledman, J., ... & Webb, E. E.  
820 (2021). Tundra Underlain By Thawing Permafrost Persistently Emits Carbon to the  
821 Atmosphere Over 15 Years of Measurements. *Journal of Geophysical Research:*  
822 *Biogeosciences*, 126(6), e2020JG006044.  
823 <https://doi.org/10.1029/2020JG006044>

824 Shen, M., Piao, S., Jeong, S. J., Zhou, L., Zeng, Z., Ciais, P., et al. (2015). Evaporative cooling  
825 over the Tibetan Plateau induced by vegetation growth. *Proceedings of the National*  
826 *Academy of Sciences*, 112(30), 9299-9304.  
827 <https://doi.org/10.1073/pnas.1504418112>

828 Shipley, B. (2016). *Cause and correlation in biology: A user's guide to path analysis, Structural*  
829 *equations and causal inference with R*. Cambridge University Press.

830 Starr, G., & Oberbauer, S. F. (2003). Photosynthesis of arctic evergreens under snow:  
831 implications for tundra ecosystem carbon balance. *Ecology*, 84(6), 1415-1420.  
832 <https://doi.org/10.1890/02-3154>

833 Thornley, J. H., & Johnson, I. R. (1990). *Plant and crop modelling*. Oxford: Clarendon.

834 Trucco, C., Schuur, E. A., Natali, S. M., Belshe, E. F., Bracho, R., & Vogel, J. (2012). Seven-  
835 year trends of CO<sub>2</sub> exchange in a tundra ecosystem affected by long-term permafrost  
836 thaw. *Journal of Geophysical Research: Biogeosciences*, 117(G2).  
837 <https://doi.org/10.1029/2011JG001907>

838 Ueyama, M., Iwata, H., & Harazono, Y. (2014). Autumn warming reduces the CO<sub>2</sub> sink of a  
839 black spruce forest in interior Alaska based on a nine-year eddy covariance  
840 measurement. *Global Change Biology*, 20(4), 1161-1173.  
841 <https://doi.org/10.1111/gcb.12434>

842 Vickers, D., & Mahrt, L. (1997). Quality control and flux sampling problems for tower and  
843 aircraft data. *Journal of Atmospheric and Oceanic Technology*, 14(3), 512-526.  
844 [https://doi.org/10.1175/1520-0426\(1997\)014%3C0512:QCAFSP%3E2.0.CO;2](https://doi.org/10.1175/1520-0426(1997)014%3C0512:QCAFSP%3E2.0.CO;2)

845 Virkkala, A. M., Aalto, J., Rogers, B. M., Tagesson, T., Treat, C. C., Natali, S. M., ... & Luoto, M.  
846 (2021). Statistical upscaling of ecosystem CO<sub>2</sub> fluxes across the terrestrial tundra and  
847 boreal domain: regional patterns and uncertainties. *Global change biology*.  
848 <https://doi.org/10.1111/gcb.15659>

849 Webb, E. E., Schuur, E. A., Natali, S. M., Oken, K. L., Bracho, R., Krapek, J. P., et al. (2016).  
850 Increased wintertime CO<sub>2</sub> loss as a result of sustained tundra warming. *Journal of*  
851 *Geophysical Research: Biogeosciences*, 121(2), 249-265.  
852 <https://doi.org/10.1002/2014JG002795>

853 Wei, D., Qi, Y., Ma, Y., Wang, X., Ma, W., Gao, T., Huang, L., Zhao, H., Zhang, J., Wang, X.  
854 (2021). Plant uptake of CO<sub>2</sub> outpaces losses from permafrost and plant respiration on the  
855 Tibetan Plateau. *Proceedings of the National Academy of Sciences*, 118 (33),  
856 e2015283118. <https://doi.org/10.1073/pnas.2015283118>

857 Wickland, K. P., Jorgenson, M. T., Koch, J. C., Kanevskiy, M., & Striegl, R. G. (2020). Carbon  
858 Dioxide and Methane Flux in a Dynamic Arctic Tundra Landscape: Decadal-Scale  
859 Impacts of Ice Wedge Degradation and Stabilization. *Geophysical Research*  
860 *Letters*, 47(22), e2020GL089894.  
861 <https://doi.org/10.1029/2020GL089894>

862 Wilczak, J. M., Oncley, S. P., & Stage, S. A. (2001). Sonic anemometer tilt correction  
863 algorithms. *Boundary-layer meteorology*, 99(1), 127-150.



- 864 <https://doi.org/10.1023/A:1018966204465>
- 865 Wu, Q., & Zhang, T. (2010). Changes in active layer thickness over the Qinghai-Tibetan Plateau  
866 from 1995 to 2007. *Journal of Geophysical Research: Atmospheres*, 115(D9).
- 867 <https://doi.org/10.1029/2009JD012974>
- 868 Wu, Q., Hou, Y., Yun, H., & Liu, Y. (2015). Changes in active-layer thickness and near-surface  
869 permafrost between 2002 and 2012 in alpine ecosystems, Qinghai-Xizang (Tibet) Plateau,  
870 China. *Global and Planetary Change*, 124, 149-155.
- 871 <https://doi.org/10.1016/j.gloplacha.2014.09.002>
- 872 Yao, T., Xue, Y., Chen, D., Chen, F., Thompson, L., Cui, P., et al. (2019). Recent third pole's  
873 rapid warming accompanies cryospheric melt and water cycle intensification and  
874 interactions between monsoon and environment: Multidisciplinary approach with  
875 observations, modeling and analysis. *Bulletin of the American Meteorological*  
876 *Society*, 100(3), 423-444.
- 877 <https://doi.org/10.1175/BAMS-D-17-0057.1>
- 878 Yun, H., Wu, Q., Zhuang, Q., Chen, A., Yu, T., Lyu, Z., et al. (2018). Consumption of  
879 atmospheric methane by the Qinghai-Tibet Plateau alpine steppe ecosystem. *The*  
880 *Cryosphere*, 12(9), 2803-2819.
- 881 <https://doi.org/10.5194/tc-12-2803-2018>
- 882 Zhang, R., Su, F., Jiang, Z., Gao, X., Guo, D., Ni, J., et al. (2015). An overview of projected  
883 climate and environmental changes across the Tibetan Plateau in the 21st  
884 century. *Chinese Science Bulletin*, 60(32), 3036-3047.
- 885 <https://doi.org/10.1360/N972014-01296>
- 886 Zhang, T., Zhang, Y., Xu, M., Zhu, J., Chen, N., Jiang, Y., et al. (2018). Water availability is  
887 more important than temperature in driving the carbon fluxes of an alpine meadow on the  
888 Tibetan Plateau. *Agricultural and Forest Meteorology*, 256, 22-31.
- 889 <https://doi.org/10.1016/j.agrformet.2018.02.027>
- 890 Zhang, W., Jansson, P. E., Schurgers, G., Hollesen, J., Lund, M., Abermann, J., et al. (2018).  
891 Process-oriented modeling of a high Arctic tundra ecosystem: Long-term carbon budget  
892 and ecosystem responses to interannual variations of climate. *Journal of Geophysical*  
893 *Research: Biogeosciences*, 123(4), 1178-1196.
- 894 <https://doi.org/10.1002/2017JG003956>



895 Zhou, Y., Guo D., Qiu G., Cheng G., & Li S. (2001). Geocryology in China. *Permafrost and*  
896 *Periglacial Processes*, 12(3), 315-322.

897 Zhu, J., Zhang, F., Li, H., He, H., Li, Y., Yang, Y., et al. (2020). Seasonal and Interannual  
898 Variations of CO<sub>2</sub> Fluxes Over 10 Years in an Alpine Wetland on the Qinghai-Tibetan  
899 Plateau. *Journal of Geophysical Research: Biogeosciences*, 125(11), e2020JG006011.  
900 <https://doi.org/10.1029/2020JG006011>

901 Zhu, Q., Iversen, C. M., Riley, W. J., Slette, I. J., & Vander Stel, H. M. (2016). Root traits  
902 explain observed tundra vegetation nitrogen uptake patterns: Implications for trait-based  
903 land models. *Journal of Geophysical Research: Biogeosciences*, 121(12), 3101-3112.  
904 <https://doi.org/10.1002/2016JG003554>

905

## 906 **Acknowledgments**

907 This work was facilitated in part by support provided by the following programs: this study was  
908 funded by the Scientific Instrument Developing Project of the Chinese Academy of Sciences,  
909 Grant No. YJKYYQ20190012 and the National Natural Science Foundation of China  
910 (41501083). We acknowledge Opening Research Foundation of State Key Laboratory of Frozen  
911 Soil Engineering, Chinese Academy of Sciences (SKLFSE201812 and SKLFSE201702). Hanbo  
912 Yun acknowledges the Strategic Priority Research Program of the Chinese Academy of Sciences  
913 (Grant No. XDA19070504) and National Cryosphere Desert Data Center, Northwest Institute of  
914 Eco-Environment and Resources, Chinese Academy of Sciences. Qing Zhu was supported by the  
915 Reducing Uncertainties in Biogeochemical Interactions through Synthesis and Computation  
916 (RUBISCO) Scientific Focus Area, which is sponsored by the Earth and Environmental Systems  
917 Modeling (EESM) Program under the Office of Biological and Environmental Research of the  
918 US Department of Energy Office of Science. Yang Qu thanks the School of Urban and Regional  
919 Science, East China Normal University (Research on Asian Water Tower Changes 13902-  
920 412125-20018/005). Wenxin Zhang was supported by the Swedish Research Council VR starting  
921 grant 2020-0533 and the Swedish National Space Agency project grant 209/19 and Bo Elberling  
922 by the Danish National Research Foundation (CENPERM DNRF100). We would like to thank  
923 Yongzhi Liu, Guilong Wu, Ji Chen and Guojun Liu for their tremendous help in collecting field  
924 data over all these years. Thanks to Professor Per-Erik Jansson for providing assistance with the  
925 non-growing season data analysis. The data generated in this study will be freely available on the  
926 Electronic Research Data Archive at the University of Copenhagen  
927 (<https://sid.erda.dk/sharelink/dgC5Qppkdj>, Data ID: dgC5Qppkdj) or the National Cryosphere  
928 Desert Data Center, Northwest Institute of Eco-Environment and Resources, Chinese Academy

929 of Sciences (<http://www.ncdc.ac.cn/portal/science/list/2>).

930

931 **Supplementary information**

- 932 1. **Supplementary Table 1.** Relationship between accumulated weekly net ecosystem exchange  
933 (NEE) and environment factors on annual, growing season, non-growing season (N-  
934 Growing Season) across 2010-2020.
- 935 2. **Supplementary Figure S1** Geographic locations of Beilu'He on the Tibetan Plateau (a) and  
936 eddy covariance observation field (b), the inset shows the automatic chamber of Li-Cor  
937 8100.
- 938 3. **Supplementary Figure S2.** Temporal changes in sum snowfall (a) and snow cover days (b)  
939 during the end of the non-growing season and the start of the growing season (1<sup>st</sup> March  
940 to 15<sup>th</sup> June) from 2011 to 2020.
- 941 4. **Supplementary Figure S3.** Accumulative net ecosystem exchange (NEE) during the end of  
942 the non-growing season and the start of the growing season (1<sup>st</sup> March to 15<sup>th</sup> June)  
943 measured by eddy covariance from 2011 to 2020 (a) and automatic chamber from 2013 to  
944 2020 (b).
- 945 5. **Supplementary Figure S4.** Relationship of net ecosystem exchange (NEE) with  
946 environmental properties, sum snowfall (a), snow cover days (b), Tsoil of 0-30 cm (c),  
947 SWC of 0-30 cm (d), VPD (e) and ALT (f) in the alpine steppe during the end of the non-  
948 growing season and the start of the growing season (1<sup>st</sup> March to 15<sup>th</sup> June) from 2011 to  
949 2020.